UNIVERSITY
OF TRENTO

DEPARTMENT OF INFORMATION AND COMMUNICATION TECHNOLOGY

38050 Povo – Trento (Italy), Via Sommarive 14
http://www.dit.unitn.it

EFFECTIVE EXPLOITATION OF THE *A-PRIORI* INFORMATION THROUGH A MICROWAVE IMAGING PROCEDURE BASED ON THE SMW FOR NDE/NDT APPLICATIONS

M. Benedetti, M. Donelli, G. Franceschini, M. Pastorino, and A. Massa

May 2005

Technical Report DIT-05-006

Effective Exploitation of the *A-Priori* Information through a Microwave Imaging Procedure based on the SMW for NDE/NDT Applications

Manuel Benedetti,* Massimo Donelli,* Gabriele Franceschini,* Matteo Pastorino,** *Senior Member, IEEE*, and Andrea Massa,* *Member, IEEE*

* Department of Information and Communication Technologies,
University of Trento, Via Sommarive 14, 38050 Trento - Italy
Tel. +39 0461 882057, Fax +39 0461 882093
E-mail: *andrea.massa@ing.unitn.it*,
{*manuel.benedetti*, *massimo.donelli*, *gabriele.franceschini*}*@dit.unitn.it*

** Department of Biophysical and Electronic Engineering,
University of Genoa, Via Opera Pia 11/A, 16145 Genoa - Italy
Tel. +39 010 3532242, Fax +39 010 3532245
E-mail: *pastorino@dibe.unige.it*

Effective Exploitation of the *A-Priori* Information through a Microwave Imaging Procedure based on the SMW for NDE/NDT Applications

Manuel Benedetti,* Massimo Donelli,* Gabriele Franceschini,* Matteo Pastorino,** *Senior Member, IEEE*, and Andrea Massa,* *Member, IEEE*

Abstract

This paper presents an innovative microwave technique, which is suitable for the detection of defects in non-destructive-test and non-destructive-evaluation (NDT/NDE) applications where a lot of *a-priori* information is available. The proposed approach is based on the equations of the inverse scattering problem, which are solved by means of a minimization procedure based on a Genetic Algorithm (GA). To reduce the number of problem unknowns, the available *a-priori* information is efficiently exploited by introducing an updating procedure for the electric field computation based on the Sherman-Morrison-Woodbury (SMW) formula. The results of a representative set of numerical experiments as well as comparisons with state-of-the-art methods are reported. They confirm the effectiveness, the feasibility, and the robustness of the proposed approach, which shows some interesting features by a computational point-of-view, as well.

Key-words: Nondestructive Testing and Evaluation, Microwave Imaging, Sherman-Morrison-Woodbury Formula, Genetic Algorithms.

1 Introduction

In general, microwave imaging of dielectric objects is an expensive computational process, because of the great number of unknowns and some negative features of the related inverse problem, such as ill-positioning and non-linearity. However, testing an object for evaluating the presence of a defect allows us to reduce the computational complexity by fully exploiting the (generally) available *a-priori* information concerning the unperturbed structure [1]. In some previous works [2]-[4], such a problem has been faced by parameterizing an anomaly such a crack in order to reduce the dimension of the search space. In particular, the most significant features of the unknown defect (i.e., position and dimensions) have been assumed as the parameters to be retrieved. To deal with non-linearity, the inverse scattering problem has been reformulated as an optimization procedure solved through a GA-based technique by defining a suitable cost function to be minimized. The convergence of the proposed algorithm has been reached after a non-negligible number of iterations strictly related to the required spatial resolution accuracy.

Recently, an improved approach, still based on a GA optimization procedure, has been presented in [5]. In such a case, the investigation domain has been limited to the area of the unknown defect, which belongs to an inhomogeneous space (the host medium without the defect and the external background). However, although the dimension of the search space has been further reduced, such an approach too requires an electric field estimation only partially related to the crack features and it does not fully exploit the relationship between the dielectric distribution and scattered fields.

Therefore, to overcome such a drawback, this work describes a new approach allowing the computational resources be fully spent for the crack localization and dimensioning. Essentially, the final aim is to estimate in a faster and more effective way the electric field distribution in the investigation domain starting from the geometric features of the defect retrieved during the iterative reconstruction process. Consequently, the arising reduction of the number of unknowns leads to an increase of the convergence rate and to

an improvement of the reconstruction accuracy.

The manuscript is organized in six sections. In Section 2, the mathematical formulation of the approach will be presented by detailing the numerical procedure for the computation of electric field in the investigation domain. Moreover, two different implementations will be described in Section 3. In Section 4, the computational improvement and the crack-detection efficiency of the method will be assessed through selected numerical results. Some remarks, arising from a comparative study (with other NDE/NDT methods), will be reported in Section 5. Finally, some conclusions will be drawn in Section 6.

2 Mathematical Formulation

Let us consider the two-dimensional geometry shown in Fig. 1, where the structure under test belongs to the region called *investigation domain*, D_{inv}. The background consists of a homogeneous external medium. The investigation domain is illuminated by V sources, which radiate known incident electric fields $\underline{E}^v_{inc}$, $v = 1, \ldots, V$ at the working frequency f_0. The electric field $\underline{E}^v_{tot}$, due to the interaction between the incident field and the dielectric distribution of the investigation domain, is collected in a set of M receivers located at certain measurement points in the *observation domain* D_{obs}. Let us assume a TM-polarization and a plane wave illumination, then the electric field turns out to be parallel to the axis of the cylindrical scatterer ($\underline{E}^v_{inc} = E^v_{inc}(x, y)\,\underline{\hat{z}}$) and the problem can be formulated in scalar form. Thus, by considering the point-matching version of the Moment Method (MoM) [6] and partitioning D_{inv} is partitioned into N equal sub-domains centered at (x_n, y_n), $n = 1, \ldots, N$, the scattering equations can be expressed in matrix form as follows

$$[E^v_{scatt}] = [G_{ext}]\,[\tau]\,[E^v_{tot}] \tag{1}$$

$$[E^v_{inc}] = [E^v_{tot}] - [G_{int}]\,[\tau]\,[E^v_{tot}] \tag{2}$$

where

- $[E^v_{scatt}]$ is a $M \times 1$ matrix whose m-th element is given by $E^v_{scatt}(x_m,\, y_m) = E^v_{tot}(x_m,\, y_m) - E^v_{inc}(x_m,\, y_m)$, $(x_m,\, y_m) \in D_{obs}$;

- $[E^v_{inc}]$ and $[E^v_{tot}]$ are $N \times 1$ matrices whose n-th elements are given by $E^v_{inc}(x_n,\, y_n)$ and $E^v_{tot}(x_n,\, y_n)$, $(x_n,\, y_n) \in D_{inv}$, respectively;

- $[G_{ext}]$ is the external Green's matrix [7] of dimension $M \times N$, while $[G_{int}]$ is the $N \times N$ internal Green's matrix [7];

- $[\tau]$ is a $N \times N$ diagonal matrix whose elements are given by $\tau_{ns} = \delta_{ns}\tau(x_n,\, y_n)$, $\delta_{ns} = 1$ if $n = s$ and $\delta_{ns} = 0$ otherwise [$\tau(x, y) \triangleq \varepsilon(x, y) - 1 - j\frac{\sigma(x,y)}{2\pi f_0 \varepsilon_0}$, $\varepsilon(x, y)$ and $\sigma(x, y)$ being the dielectric constant and conductivity, respectively].

Starting from such a mathematical description, the inversion procedure for NDE/NDT applications is aimed at detecting the presence of a crack in the host medium, whose cross-section defines the area of investigation. By neglecting the *a-priori* information on the unperturbed geometry (generally, available in several NDE/NDT applications concerned with the defect detection), the problem unknowns would be the object function $\tau(x_n,\, y_n)$ and the total electric field $E^v_{tot}(x_n,\, y_n)$ at each pixel of D_{inv} $(n = 1,\, \ldots,\, N)$. Thus, due to the large number of unknowns, even though in presence of a non-negligible nonlinearity, it could be profitable to solve such a standard inverse scattering problem through CG-FFT methods [8].

Fortunately, by taking into account the *a-priori* information available in the crack-detection NDE/NDT problem, it is possible to notably reduce the search space, modeling the defect as an unknown small "object" in a known host medium. Under such a hypothesis, let us approximate this "object" by means of a homogeneous rectangular void centered at $(x_0,\, y_0)$ $[(x_0,\, y_0) \in \{(x_n,\, y_n),\, n = 1,\, \ldots,\, N\}]$, characterized by a length L, a width W, and an orientation θ (Fig. 1). In such a way, $\tau(x_n,\, y_n)$ is a function of the features of the

crack $\underline{\psi} = \{x_0,\, y_0,\, L,\, W,\, \theta\}$:

$$\tau\left(x_n,\, y_n\right) = \begin{cases} \tau_0 & if \quad X \in \left[-\frac{L}{2}, \frac{L}{2}\right] \; and \; Y \in \left[-\frac{W}{2}, \frac{W}{2}\right] \\ \tau_{(U)}\left(x_n,\, y_n\right) & otherwise \end{cases} \tag{3}$$

where

- τ_0 is the value of the object function of the defect;
- $\tau_{(U)}\left(x_n,\, y_n\right)$ is the value of the object function at the n-th cell of the unperturbed host medium;
- $X = (x_n - x_0)\, cos\theta + (y_n - y_0)\, sin\theta$ and $Y = (x_n - x_0)\, sin\theta + (y_n - y_0)\, cos\theta$;
- $L,\; W,\; \theta$ are assumed to belong to finite sets of values: $L \in \{L_i;\, i = 1,\, ...\,, \ell\}$, $W \in \{W_j;\, j = 1,\, ...\,, w\}$, and $\theta \in \{\theta_h;\, h = 1,\, ...\,, t\}$, $\theta_h = h\Delta\theta$.

Therefore, if $E^v_{tot}\left(x_n, y_n\right),\; n = 1,\, ...\,, N$, is expressed as a function of $\underline{\psi}$, the solution of the scattering problem can be obtained as

$$\underline{\psi}_{opt} = arg\left\{min_{\underline{\psi}}\left[\Theta\left(\underline{\psi}\right)\right]\right\} \tag{4}$$

being

$$\Theta\left(\underline{\psi}\right) = \frac{\sum_{v=1}^{V} \left\|\left[E^v_{scatt}\right] - \left[G_{ext}\right]\left[\tau\right]\left[E^v_{tot}\right]\right\|^2}{\sum_{v=1}^{V} \left\|\left[E^v_{scatt}\right]\right\|^2} + \frac{\sum_{v=1}^{V} \left\|\left[E^v_{inc}\right] - \left\{\left[E^v_{tot}\right] - \left[G_{int}\right]\left[\tau\right]\left[E^v_{tot}\right]\right\}\right\|^2}{\sum_{v=1}^{V} \left\|\left[E^v_{inc}\right]\right\|^2} \tag{5}$$

where $\left[E^v_{tot}\right] = \Im\left\{\underline{\psi}\right\}$ and $\left[\tau\right] = \aleph\left\{\underline{\psi}\right\}$ according to Eq. (3).

Due to the nonlinearity of $\Theta\left(\underline{\psi}\right)$ and the reduced number of problem unknowns, the minimization of $\Theta\left(\underline{\psi}\right)$ is carried out by means of a suitable version of a genetic algorithm [9][10]. This multiple-agent stochastic optimizer demonstrated to be very effective in dealing with reduced and nonlinear search spaces where deterministic methodologies generally failed yielding wrong solutions corresponding to local minima of the functional

to be minimized. According to the implementation described in [2] and by using binary genetic operators, a sequence of populations of trial solutions $\left\{\underline{\psi}_{q,k},\ q = 1,\ ...\ , Q\right\}$ (being k the iteration index, $k = 1,\ ....\ , K$, and q the index of the trial solution in the population) is generated, whose optimal individual converges to the minimum of (5), $\underline{\psi}_{opt} = arg\left[min_k\left(min_q\left(\Theta\left\{\underline{\psi}_{q,k}\right\}\right)\right)\right]$. Because of the integer-valued unknowns (after discretization, the coordinates of the center of the defect are assumed as integer parameters, too), $\underline{\psi}$ is coded in a binary concatenated chromosome (Figure 2) in which L, W, θ, x_0, and y_0 are coded in binary strings of $I = log_2\ell$ bits, $J = log_2 w$, $T = log_2 t$, and $C = log_2\sqrt{N}$, respectively.

3 Outline of the SMW-based Method for Field Prediction

As far as the computation of the unknown electric field values ($[E^v_{tot}] = \Im\left\{\underline{\psi}\right\}$) is concerned, a method based on the Sherman-Morrison-Woodbury formula for matrix inversion [11] is considered.

Let us assume that the perturbed geometry (i.e., the host medium with the defect) consists of P ($P < N$) discretization sub-domains different from a known reference configuration (characterized by a known distribution $\tau_{(ref)}\left(x_n,\ y_n\right),\ n = 1,\ ...\ , N$). Moreover, let us introduce two $N \times N$ matrices, $[\Omega]$ and $[\Upsilon]$, which are related to the perturbed and the reference geometry, and given by

$$[\Omega] = \{[I] - [G_{int}]\,[\tau]\} \tag{6}$$

$$[\Upsilon] = \left\{[I] - [G_{int}]\left[\tau_{(ref)}\right]\right\} \tag{7}$$

where

$$\left[\tau_{(ref)}\right] = \begin{bmatrix} \tau_{(ref)}\left(x_1,\, y_1\right) & \cdots & 0 \\ \vdots & \ddots & \vdots \\ 0 & \cdots & \tau_{(ref)}\left(x_N,\, y_N\right) \end{bmatrix}$$

and the entries of $[\tau]$ are functions of $\underline{\psi}$ according to the relationship defined in (3); $[I]$ is the identity matrix. Thus, the unknown total electric field in D_{inv} can be computed by using a computationally expensive matrix inversion as $[E^v_{tot}] = [\Omega]^{-1}[E^v_{inc}]$ (in the following we will refer to such a procedure as "Direct Algorithm"). On the other hand, the computational cost reduces, if $[\Upsilon]^{-1}$ is available and when the SMW formula is used

$$[\Omega]^{-1} = [\Upsilon]^{-1} + [\Upsilon]^{-1}[C]\left\{[I] - [F]^T[\Upsilon]^{-1}[C]\right\}^{-1}[F]^T[\Upsilon]^{-1} \tag{8}$$

where

- $[\Omega] - [\Upsilon] = -[C][F]^T$
- $[C]$ is an $N \times P$ matrix whose columns are the P non-zero columns in $[\Omega] - [\Upsilon]$;
- $[F]$ is an $N \times P$ matrix whose p-th column, $p = 1, \ldots, P$ has the value 1 at its j_p-th entry and 0 otherwise ($j_1, \ldots, j_P$, being the P non-zero columns in $[\Omega] - [\Upsilon]$).

Then, two different versions of the approach based on the SMW for the iterative estimation of $[E^v_{tot}]$ can be considered. The main difference lies in the choice of the reference configuration for the dielectric profile in the investigation domain. They will be detailed in the next sub-sections.

3.1 SMW "Unperturbed Configuration" (SMW_U)

In such a version, the unperturbed geometry is assumed as reference model ($\tau_{(ref)}\left(x_n,\, y_n\right) = \tau_{(U)}\left(x_n,\, y_n\right)$, $n = 1, \ldots, N$) and

$$[\Upsilon] = \left\{[I] - [G_{int}]\left[\tau_{(U)}\right]\right\}. \tag{9}$$

Therefore, the reference matrix $[\Upsilon]$, which depends on the known unperturbed configuration and not at all on the defect, can be computed off-line and only once during the initialization phase of the iterative minimization ($k = 1$).

Then, for the q-th trial solution at the k-th iteration ($k > 1$), $\underline{\psi}_{q,k}$, the corresponding perturbed matrix turns out to be

$$[\Omega]_{q,k} = \left\{ [I] - [G_{int}] [\tau]_{q,k} \right\} \qquad q = 1, \ldots, Q \tag{10}$$

where the sub-scripts q and k denote quantities (matrices or scalars) related to $\underline{\psi}_{q,k}$. In particular, $[\tau]_{q,k}$ is a function of $\underline{\psi}_{q,k} = \left\{ x_0\rfloor_{q,k}\,,\ y_0\rfloor_{q,k}\,,\ L\rfloor_{q,k}\,,\ W\rfloor_{q,k}\,,\ \theta\rfloor_{q,k} \right\}$ through (3). Successively, Eq. (8) is applied to compute $[\Omega]^{-1}_{q,k}$

$$[\Omega]^{-1}_{q,k} = [\Upsilon]^{-1} + [\Upsilon]^{-1} [C]_{q,k} \left\{ [I] - [F]^T_{q,k} [\Upsilon]^{-1} [C]_{q,k} \right\}^{-1} [F]^T_{q,k} [\Upsilon]^{-1} \qquad q = 1, \ldots, Q \tag{11}$$

to give an estimation of the unknown electric field in the investigation domain

$$[E^v_{tot}]_{q,k} = [\Omega]^{-1}_{q,k} [E^v_{inc}] \tag{12}$$

concerned with the configuration $\underline{\psi}_{q,k}$ of the crack features.

3.2 SMW "Best Individual" (SMW_B)

Since a suitable GA is used as the optimization procedure, it is possible to choose as reference model at the k-th iteration $\left[\tau_{(ref)}\right] = [\tau]_{opt,k-1}$, $[\tau]_{opt,k-1}$ being a function of $\underline{\psi}_{opt,k-1} = arg \left[min_q \left(\Theta \left\{ \underline{\psi}_{q,k-1} \right\} \right) \right]$ according to (3).

Therefore, the iterative updating of $[E^v_{tot}]_{q,k}$ is obtained through (12) by considering that

$$[\Upsilon]_k = \begin{cases} [I] - [G_{int}] \left[\tau_{(U)}\right] & k = 1 \\ [I] - [G_{int}] [\tau]_{opt,k-1} & k > 1 \end{cases} \tag{13}$$

and

$$[\Omega]_{q,k}^{-1} = [\Upsilon]_k^{-1} + [\Upsilon]_k^{-1} [C]_{q,k} \left\{ [I] - [F]_{q,k}^T [\Upsilon]_k^{-1} [C]_{q,k} \right\}^{-1} [F]_{q,k}^T [\Upsilon]_k^{-1} \quad q = 1, \ldots, Q \quad (14)$$

4 Numerical Validation and Comparative Assessment

In this section, the SMW-based approach will be assessed by considering a selected set of numerical simulations. Both the proposed versions of the approach will be analyzed and the achieved results will be compared with those of previous implementations, which have been denoted as FGA [2] and IGA [5], in terms of the "localization error" (δ_c), the "dimensioning error" (δ_a) (as defined in [2]), and the "field-prediction error" (ΔE_{tot}) defined as

$$\Delta E_{tot} = \left\{ \frac{1}{NV} \sum_{v=1}^{V} \sum_{n=1}^{N} \frac{\left| \left| \widehat{E_{tot}^{n,v}} \right| - \left| E_{tot}^{n,v} \right| \right|}{\left| E_{tot}^{n,v} \right|} \right\} \times 100 \quad (15)$$

where $E_{tot}^{n,v} = E_{tot}^{v}(x_n, y_n)$ and the super-script $\widehat{\ }$ indicates a reconstructed quantity.

Concerning the problem geometry, a square homogeneous cylinder of side $l = 0.8\,\lambda_0$ (λ_0 being the free-space wavelength) illuminated by a set of $V = 4$ plane-waves ($E_{inc}^{v}(x, y) = e^{-jk_0(x cos\theta_v + y sin\theta_v)}$, $\theta_v = (v-1)\frac{2\pi}{V}$) has been assumed. The scattering data have been collected in $M = 50$ measurement points equally-spaced on a circle $r = 0.64\,\lambda_0$ in radius. Moreover, D_{inv} has been discretized into $N = 256$ square sub-domains $l_{cell} = 0.05\,\lambda_0$-sided (Figure 3). Moreover, to simulate realistic environmental conditions, a noise of Gaussian-type and characterized by a fixed signal-to-noise ratio (SNR) has been added to scattering data.

Concerning the optimization procedure, the following parametric setup has been assumed: $Q = 80$, $P_m = 0.4$ (mutation probability), $P_{bm} = 0.01$ (bit-mutation probability), and $P_c = 0.7$ (crossover probability) [10]. Moreover, the iterative process has been stopped

when $K = 1000$ or if the *stationary condition* holds

$$\frac{\left| K_{const} \Theta \left\{ \underline{\psi}_{opt,k} \right\} - \sum_{h=1}^{K_{const}} \Theta \left\{ \underline{\psi}_{opt,h} \right\} \right|}{\Theta \left\{ \underline{\psi}_{opt,k} \right\}} \leq \gamma_{st} \tag{16}$$

where $\Theta_{opt,k} = \Theta \left\{ \underline{\psi}_{opt,k} \right\}$, $K_{const} = \frac{K}{50}$, and $\gamma_{st} = 3 \times 10^{-2}$.

4.1 Computational Issues

In order to evaluate the performance of the proposed approach in terms of computational costs, the following test case has been considered. An host medium, characterized by $\tau_{(U)}(x_n, y_n) = 1$, $n = 1, ..., N$, has been located in a noisy ($SNR = 15.0\, dB$) scenario. The unknown defect has been positioned in $x_0 = 0.15\, \lambda_0$ and $y_0 = 0.10\, \lambda_0$ and different values of its area have been considered to evaluate the dependence of the reconstruction process on the dimension of the problem at hand.

Figure 4 shows the plot of the required CPU-time for each iteration (t_k) and for various dimensions of the defect when the SMW_U and the SMW_B are used [Figure 4(a)]. As it can be observed, t_k for SMW_B is independent on the area of the defect A_c, while it strictly depends on the dimension of the defect when the SMW_U approach is used. Concerning the SMW_U, t_k grows as A_c increases and the approach turns out to be effective when $A_c \leq 6.25 \times 10^{-2}\, \lambda_0^2$ [Fig. 4(a)]. On the contrary, for the SMW_B, t_k is about an order in magnitude smaller than the CPU-time for the *Direct Algorithm* [Fig. 4(b)]. Moreover, it performs worse if compared with the FGA and the IGA. However, its should be pointed out that both approaches based on SMW formula require a lower number of iterations to reach the convergence [Fig. 4(b)], the length of the curve being characteristic of the required number of iterations.

Therefore, to complete the assessment of the effectiveness of the proposed implementations, it is needed to evaluate their reconstruction performance, as well. Towards this aim, different representative test cases have been considered.

4.2 Reconstruction Accuracy versus the Crack Area

By considering the same geometric arrangement of the previous example, a comparison among the reconstruction methods has been carried out in terms of error figures by varying the dimension of the defect from $A_c = 2.50 \times 10^{-3}$ up to $A_c = 2.50 \times 10^{-1}\,\lambda_0^2$ and for SNRs in the range between $2.5\,dB$ and $30.0\,dB$. Figure 5 shows the gray-scale representations of the localization error δ_c when the SMW_U [Figure 5(a)], the SMW_B [Figure 5(b)], the FGA [Figure 5(c)], and the IGA [Figure 5(d)] are used, respectively. By comparing Fig. 5(a) with Fig. 5(b), it turns out that SMW_B is more sensitive to the noise level than SMW_U, especially for the lowest values of A_c. Moreover, methods based on SMW formula outperform FGA when $A_c < 12.25 \times 10^{-2}\,\lambda_0^2$ and IGA when $A_c > 12.25 \times 10^{-2}\,\lambda_0^2$, respectively. The localization accuracy of the SMW-based techniques is further confirmed on average since, $\langle \delta_c \rangle_{SMW_U} = 2.76$ and $\langle \delta_c \rangle_{SMW_B} = 3.62$ versus $\langle \delta_c \rangle_{FGA} = 3.82$ and $\langle \delta_c \rangle_{IGA} = 3.84$.

As far as the dimensioning of the defect is concerned, the SMW_U slightly outperforms the SMW_B and the IGA approaches ($\langle \delta_a \rangle_{SMW_U} = 13.94$, $\langle \delta_a \rangle_{SMW_B} = 15.37$, and $\langle \delta_a \rangle_{IGA} = 14.69$), in particular for low noise conditions [Figs. 6(a)-(b)]. On the other hand, a larger improvement is achieved with respect to the FGA technique ($\langle \delta_a \rangle_{FGA} = 33.00$).

Finally, as expected, the SMW-based approaches notably overcome the FGA and the IGA methods in predicting the electric field induced in the investigation domain as shown in Fig. 7 and confirmed by the average values of ΔE_{tot} ($\langle \Delta E_{tot} \rangle_{SMW_U} = 5.95$, $\langle \Delta E_{tot} \rangle_{SMW_B} = 7.01$, $\langle \Delta E_{tot} \rangle_{FGA} = 31.27$, and $\langle \Delta E_{tot} \rangle_{IGA} = 12.04$).

4.3 Reconstruction Accuracy versus the Host Medium Conductivity

In the following example, the reconstruction capabilities are assessed for a lossy host medium. Towards this end, the electric conductivity of the homogeneous host medium has been varied in the range $\sigma_{(U)} \in [0.0,\ 1.0]$ and a square defect ($0.2\,\lambda_0$-sided) has been

located at $x_0 = 0.26\,\lambda_0$ and $y_0 = 0.0\,\lambda_0$.

The localization errors are reported in Figure 8 with a gray-scale representation. By comparing the results for the SMW_U and the SMW_B [Figures 8(a)-(b)], it turns out that the "best individual" implementation is more strongly affected by the value of $\sigma_{(U)}$ than its "unperturbed" counterpart. Nevertheless, SMW-based methods as well as the IGA technique show good localization properties whatever the host medium and the environment conditions as confirmed by the average values ($\langle\delta_c\rangle_{SMW_U} = 3.22$, $\langle\delta_c\rangle_{SMW_B} = 7.35$, and $\langle\delta_c\rangle_{IGA} = 4.18$). On the contrary, the defect is not satisfactorily localized when the FGA is adopted ($\langle\delta_c\rangle_{FGA} = 20.75$).

Similar conclusions hold for the estimation of the crack dimensions (Figure 9). In fact, on average, the SMW_U reaches the best results as compared with other techniques ($\langle\delta_a\rangle_{SMW_U} = 15.59$, $\langle\delta_a\rangle_{SMW_B} = 36.95$, $\langle\delta_a\rangle_{FGA} > 100.0$, and $\langle\delta_a\rangle_{IGA} = 28.14$).

Finally, once again, SMW techniques demonstrate very accurate in estimating the unknown electric field as pointed out by the values of the error figure [Figures 10(a)(b)(c)(d)] as well as on average ($\langle\Delta E_{tot}\rangle_{SMW_U} = 3.34$, $\langle\Delta E_{tot}\rangle_{SMW_B} = 8.19$, $\langle\Delta E_{tot}\rangle_{FGA} = 38.57$, and $\langle\Delta E_{tot}\rangle_{IGA} = 10.34$).

5 Final Remarks

On the basis of the computational costs and the reconstruction capabilities discussed in the previous sub-sections, a deeper comparison is performed by considering the IGA and the SMW_B approaches as representative methodologies. As a matter of fact, the "best individual" implementation of the SMW-based method is more efficient than the SMW_U technique since it allows to reduce the computational burden for any crack dimension A_c [Figures 4(d)-(e)] by keeping (or improving) the accuracy in the defect localization and dimensioning. Moreover, Figs. 5-10 pointed out that the behaviors of the error figures δ_c, δ_a, and ΔE_{tot} are very close/similar for both the SMW techniques and the corresponding average values turn out to be adequate for an accurate reconstruction.

In comparison with the IGA, SMW_B is computationally more expensive [Figure $4(e)$], although it converges faster and it is more accurate in reconstructing the perturbed scenario, mainly concerning the prediction of the electric field. To point out such properties, Figures 11 and 12 show a gray-scale representation of the discrepancy error figures: $\chi_c = \delta_c^{(IGA)} - \delta_c^{(SMW_B)}$, $\chi_a = \delta_a^{(IGA)} - \delta_a^{(SMW_B)}$, and $\chi_{E_{tot}} = \Delta E_{tot}^{(IGA)} - \Delta E_{tot}^{(SMW_B)}$ for the two analyzed test cases (Subsection 4.2 and Subsection 4.3).

As can be observed from Figure 11, IGA and SMW_B reach almost the same accuracy in locating and dimensioning the defect [Figs. $11(a)(b)$], while Figure $11(c)$ points out that the SMW_B is more efficient in the field computation, especially when the data are affected by noise.

The same conclusions can be drawn by considering the effects of $\sigma_{(U)}$. In such a case, the SMW_B approach works better when the host medium is lossy, too [Figure 12].

Finally, the last example deals with a host medium discretized into $N = 3969$ square pixels in order to confirm the effectiveness of the proposed approach in exploiting the available *a-priori* information in a larger dimension of the problem, as well. As a matter of fact, when the SMW is used, the dimension of $\underline{\psi}_{SMW}$ does not depend on the discretization of the investigation domain and the unknown electric field samples ($E_{tot}^{n,v}$, $n = 1, ..., N$, $v = 1, ..., V$) are determined through the SMW-based matrix inversion procedure starting from the estimate of $\underline{\psi}_{SMW}$.

Thus, as expected, the SMW_B keeps almost unaltered its properties in terms of reconstruction accuracy as shown in Fig. 13 where the behaviors of the error figures concerned with the crack reconstruction are reported ($A_c = 0.09\,\lambda_0^2$, $x_0 = 0.15\,\lambda_0$ and $y_0 = 0.1\,\lambda_0$). On the contrary, since the number of unknowns to be determined by means of the optimization procedure, $\underline{\psi}_{IGA} = \{x_0,\, y_0,\, L,\, W,\, \theta;\, E_{tot}^{n,v},\, n = 1, ..., N;\, v = 1, ..., V\}$, as well as the dimension of the search space directly depend on N, the effectiveness of the IGA in locating the defect significantly reduces increasing the discretization of D_{inv}.

6 Conclusions

A new technique for a microwave NDT/NDE crack-detection has been proposed. The approach, based on the Sherman-Morrison-Woodbury updating formula, fully exploit the available *a-priori* information about the unperturbed configuration. The effectiveness of the proposed approach has been assessed through a numerical analysis by considering input data affected by noise as well as dissipative host media, too. The obtained results has confirmed the capabilities of the method in locating and dimensioning the defect and in accurately estimating the distribution of the total electric inside the test area.
However, it has been observed that the allowed improvement in the reconstruction accuracy has, as a counterpart, a non-negligible increase of the computational burden cost in comparison with other approaches. Therefore, the reduction of the computational load is still an open question that will be further addressed, especially to extend the diagnostic procedure to three-dimensional configurations.

References

[1] R. Zoughi, *Microwave Testing and Evaluation.* Kluwer Academic Publishers, The Netherlands, 2000.

[2] S. Caorsi, A. Massa and M. Pastorino, "A crack identification microwave procedure based on a genetic algorithm for nondestructive testing," *IEEE Trans. Antennas Propagat.*, vol. 49, pp. 1812-1820, 2001.

[3] S. Caorsi, A. Massa, M. Pastorino, and F. Righini, "Crack detection in lossy two-dimensional structures by means of a microwave imaging approach," *Int. J. Appl. Electromagnetics Mechanics,* vol. 11, pp. 233-244, 2000.

[4] M. Pastorino, A. Massa, and S. Caorsi, "A global optimization technique for microwave nondestructive evaluation," *IEEE Trans. Instrum. Meas.,* vol. 51, pp. 666-673, 2002.

[5] S. Caorsi, A. Massa, M. Pastorino, and M. Donelli, "Improved microwave imaging procedure for nondestructive evaluations of two-dimensional structures," *IEEE Trans. Antennas Propagat.*, vol. 52, pp. 1386-1397, 2004.

[6] J. H. Richmond, "Scattering by a dielectric cylinder of arbitrary cross section shape," *IEEE Trans. Antennas Propagat.*, vol. 13, pp. 334-341, 1965.

[7] D. S. Jones, *The Theory of Electromagnetism.* Oxford, U.K.: Pergamon Press, 1964.

[8] W. C. Chew, G. L. Wang, A. A. Aydiner, and T. J. Cui, "Recent advances in nonlinear inverse scattering," *Proc. 2004 Int. Symp. Electrom. Theory* (URSI 2004), pp. 697-699, May 23-27, 2004.

[9] D. E. Goldberg, *Genetic Algorithms in Search, Optimization, and Machine Learning.* Addison-Wesley, Reading, MA, USA, 1989.

[10] J. M. Johnson and Y. Rahmat-Samii, "Genetic algorithms in engineering electromagnatics," *IEEE Trans. Antennas Propagat. Mag.,* vol. 39, pp 7-26, April 1997.

[11] E. Yip and B. Tomas, "Obtaining scattering solution for perturbed geometries and materials from moment method solutions," *ACES Journal*, pp. 95-118, 1988.

Figure Captions

- **Figure 1.** Problem geometry.
- **Figure 2.** The binary-coded chromosome.
- **Figure 3.** Discretized geometry. Square homogeneous cylinder (cross section).
- **Figure 4.** CPU times for various crack area: (a) Comparison among the SMW_U-based approach, the SMW_B-based approach and the Direct Algorithm when $A_c = 0.0625\lambda^2$ and $A_c = 0.1225\lambda^2$. (b) Comparison among the SMW_U-based approach, the SMW_B-based approach, FGA, IGA, and the Direct Algorithm when $A_c = 0.0225\lambda^2$.
- **Figure 5.** Error parameter δ_c versus the crack area for different SNR values: (a) SMW_U-based approach, (b) SMW_B-based approach, (c) FGA, and (d) IGA.
- **Figure 6.** Error parameter δ_a versus the crack area for different SNR values: (a) SMW_U-based approach, (b) SMW_B-based approach, (c) FGA, and (d) IGA.
- **Figure 7.** Error parameter ΔE_{tot} versus the crack area for different SNR values: (a) SMW_U-based approach, (b) SMW_B-based approach, (c) FGA, and (d) IGA.
- **Figure 8.** Error parameter δ_c versus $\sigma_{(U)}$ for different SNR values: (a) SMW_U-based approach, (b) SMW_B-based approach, (c) FGA, and (d) IGA.
- **Figure 9.** Error parameter δ_a versus $\sigma_{(U)}$ for different SNR values: (a) SMW_U-based approach, (b) SMW_B-based approach, (c) FGA, and (d) IGA.
- **Figure 10.** Error parameter ΔE_{tot} versus $\sigma_{(U)}$ for different SNR values: (a) SMW_U-based approach, (b) SMW_B-based approach, (c) FGA, and (d) IGA.
- **Figure 11.** Error figures ((a) χ_c, (b) χ_a, and (c) $\chi_{E_{tot}}$) versus the the crack dimension A_c and for different SNR values.

- **Figure 12.** Error figures ((a) χ_c, (b) χ_a, and (c) $\chi_{E_{tot}}$) versus the host medium conductivity $\sigma_{(U)}$ and for different SNR values.

- **Figure 13.** Behavior of (a) χ_c and (b) χ_a versus SNR when $N = 3969$ and for SMW_B and IGA.

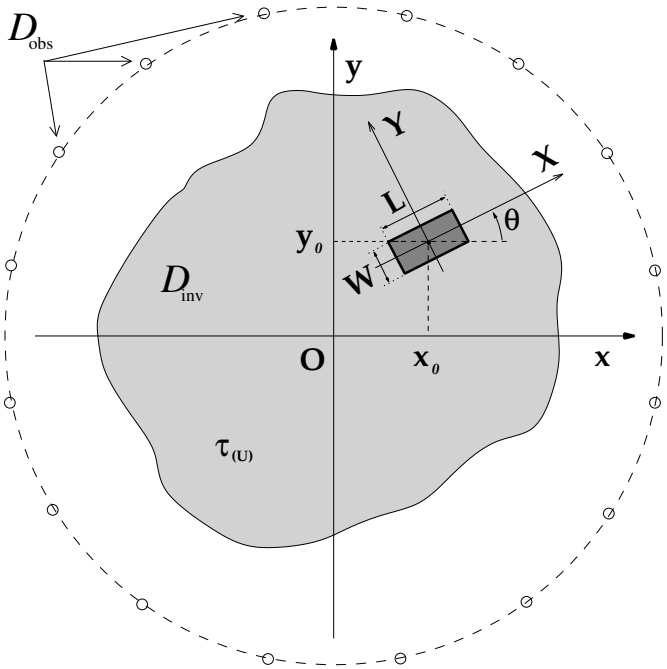

Fig. 1 - M. Benedetti *et al.*, "Effective Exploitation of the *A-Priori* Information ..."

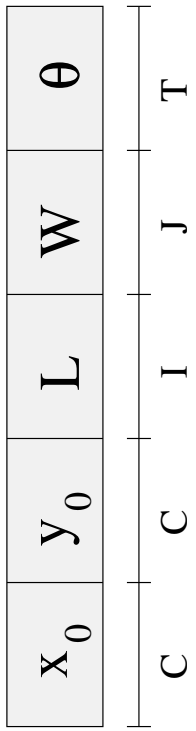

Fig. 2 - M. Benedetti *et al.*, "Effective Exploitation of the *A-Priori* Information ..."

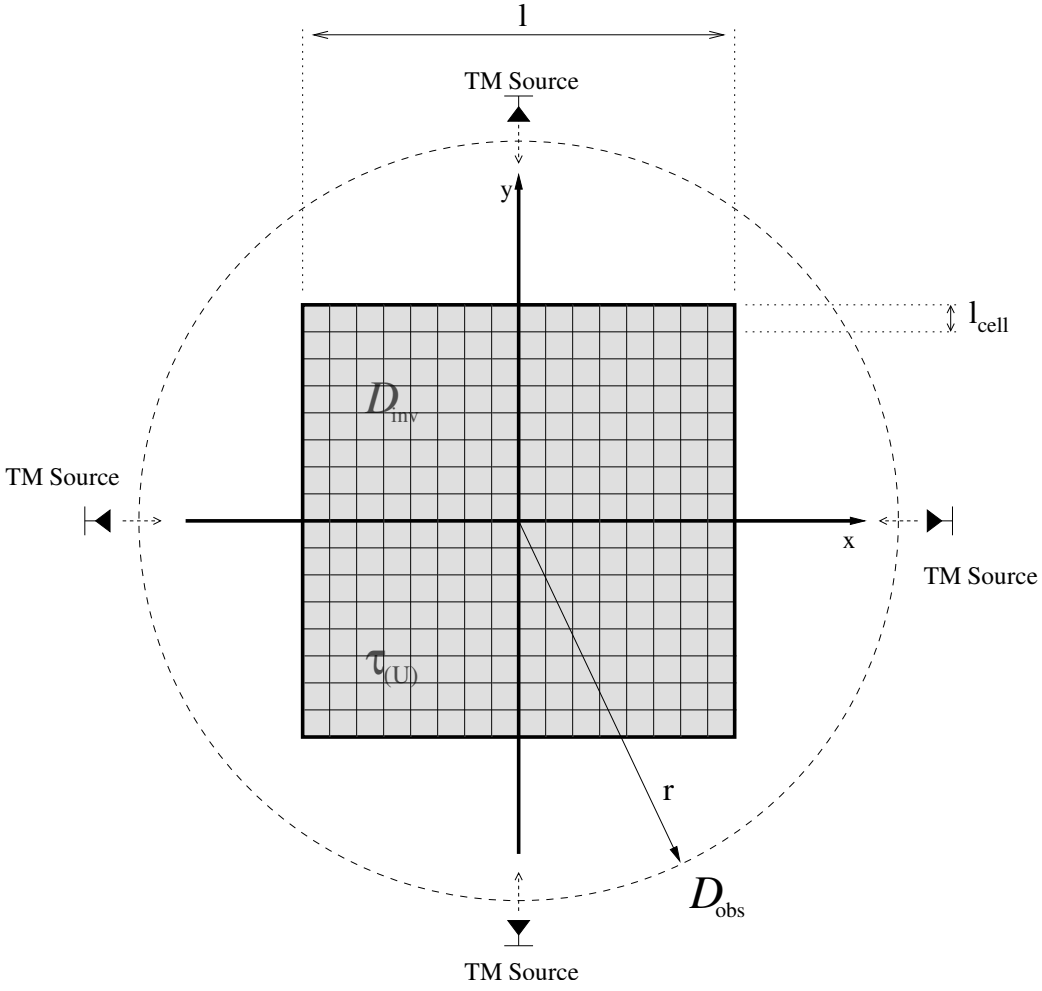

Fig. 3 - M. Benedetti *et al.*, "Effective Exploitation of the *A-Priori* Information ..."

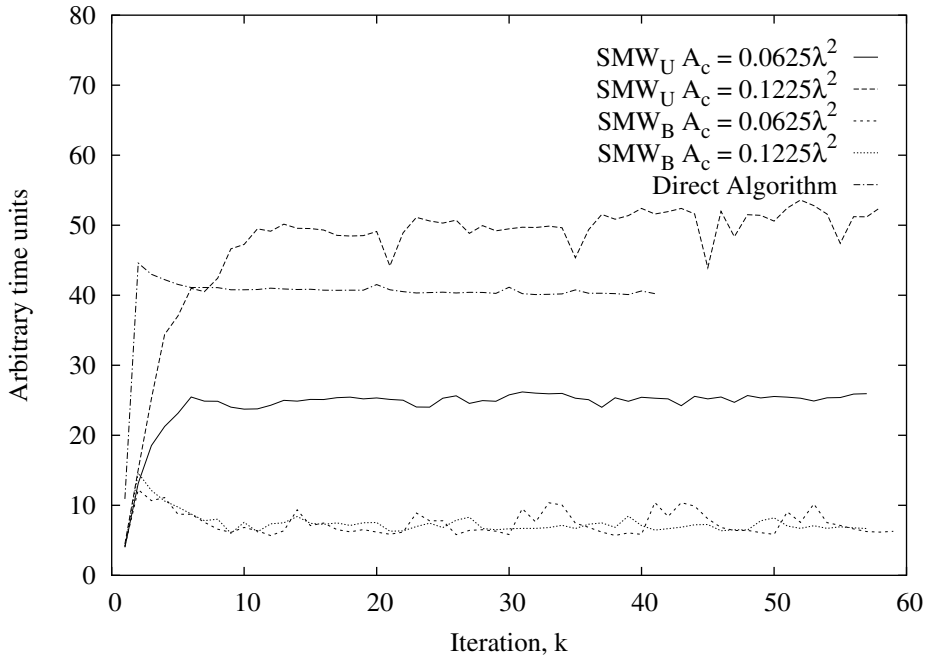

(a)

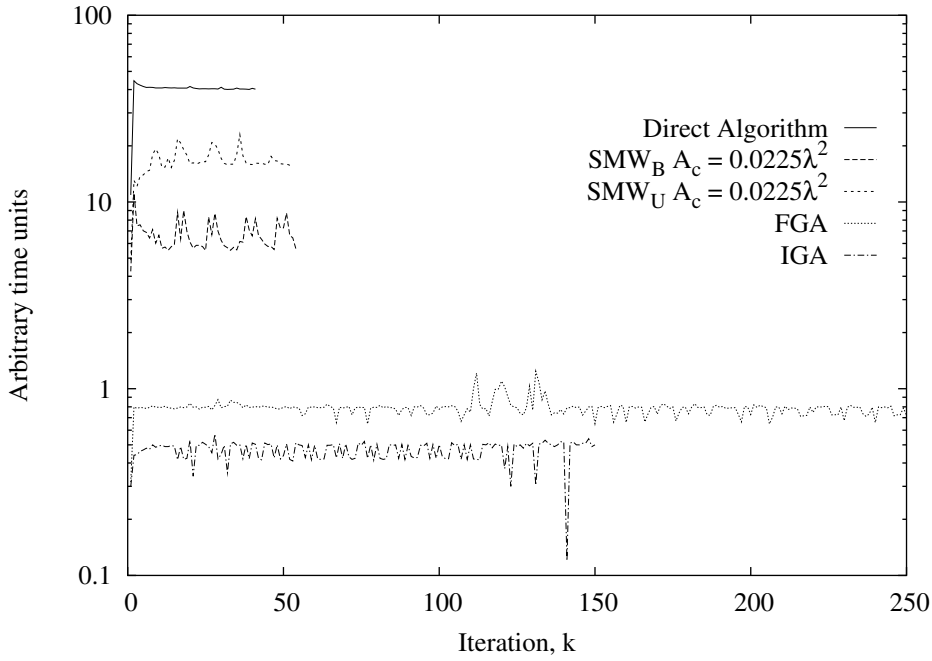

(b)

Fig. 4 - M. Benedetti *et al.*, "Effective Exploitation of the *A-Priori* Information ..."

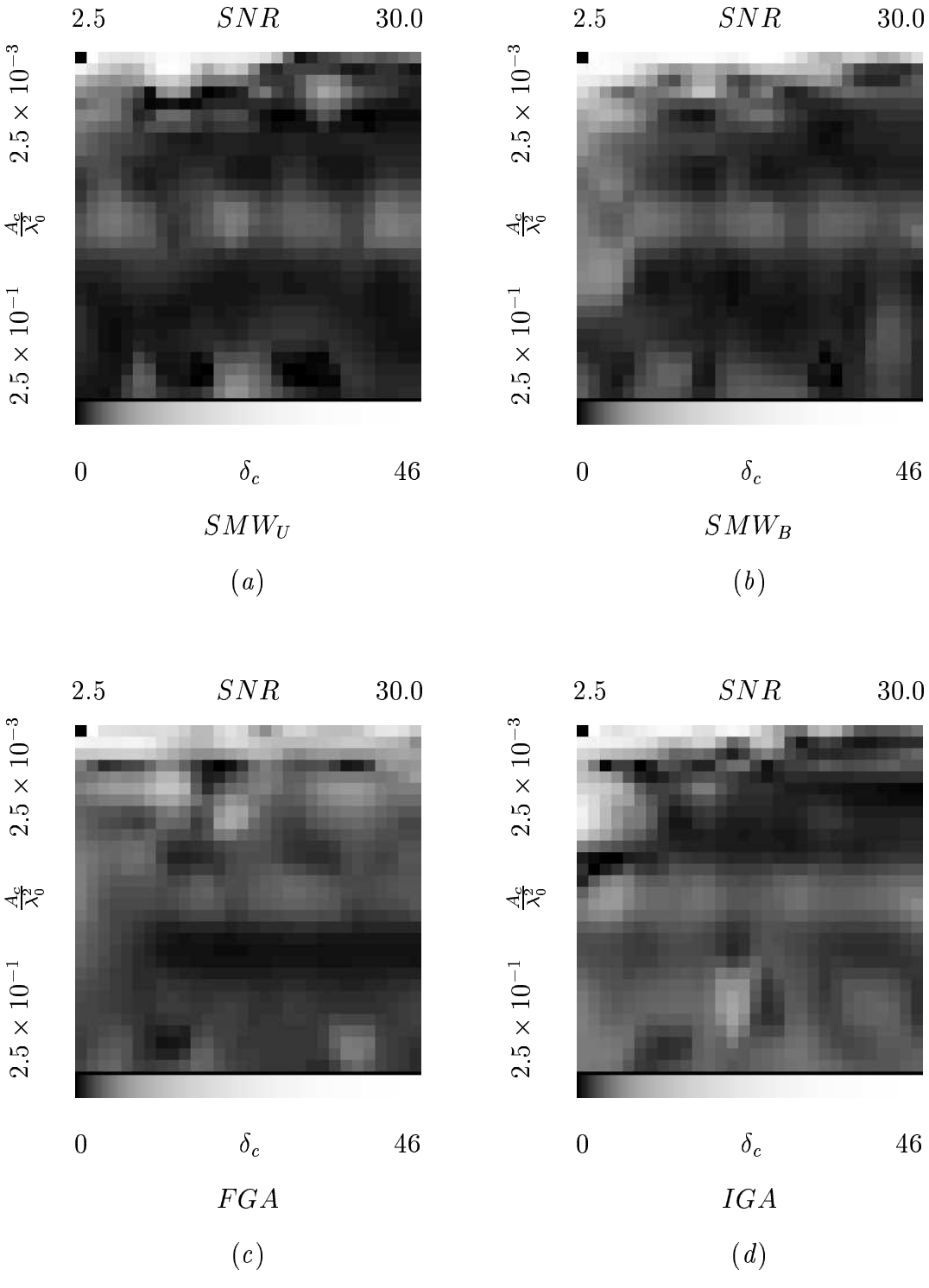

Fig. 5 - M. Benedetti *et al.*, "Effective Exploitation of the *A-Priori* Information ..."

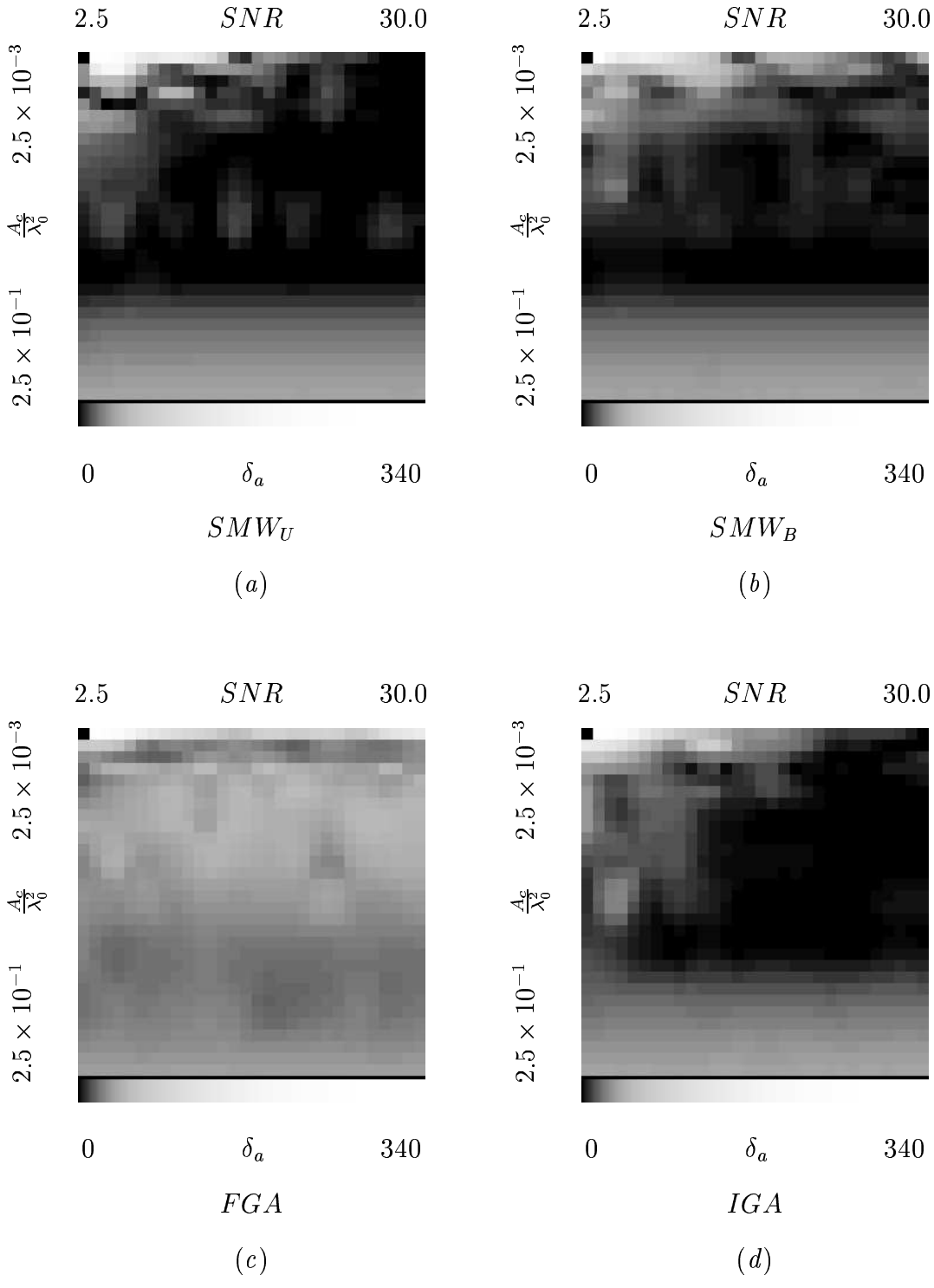

Fig. 6 - M. Benedetti *et al.*, "Effective Exploitation of the *A-Priori* Information ..."

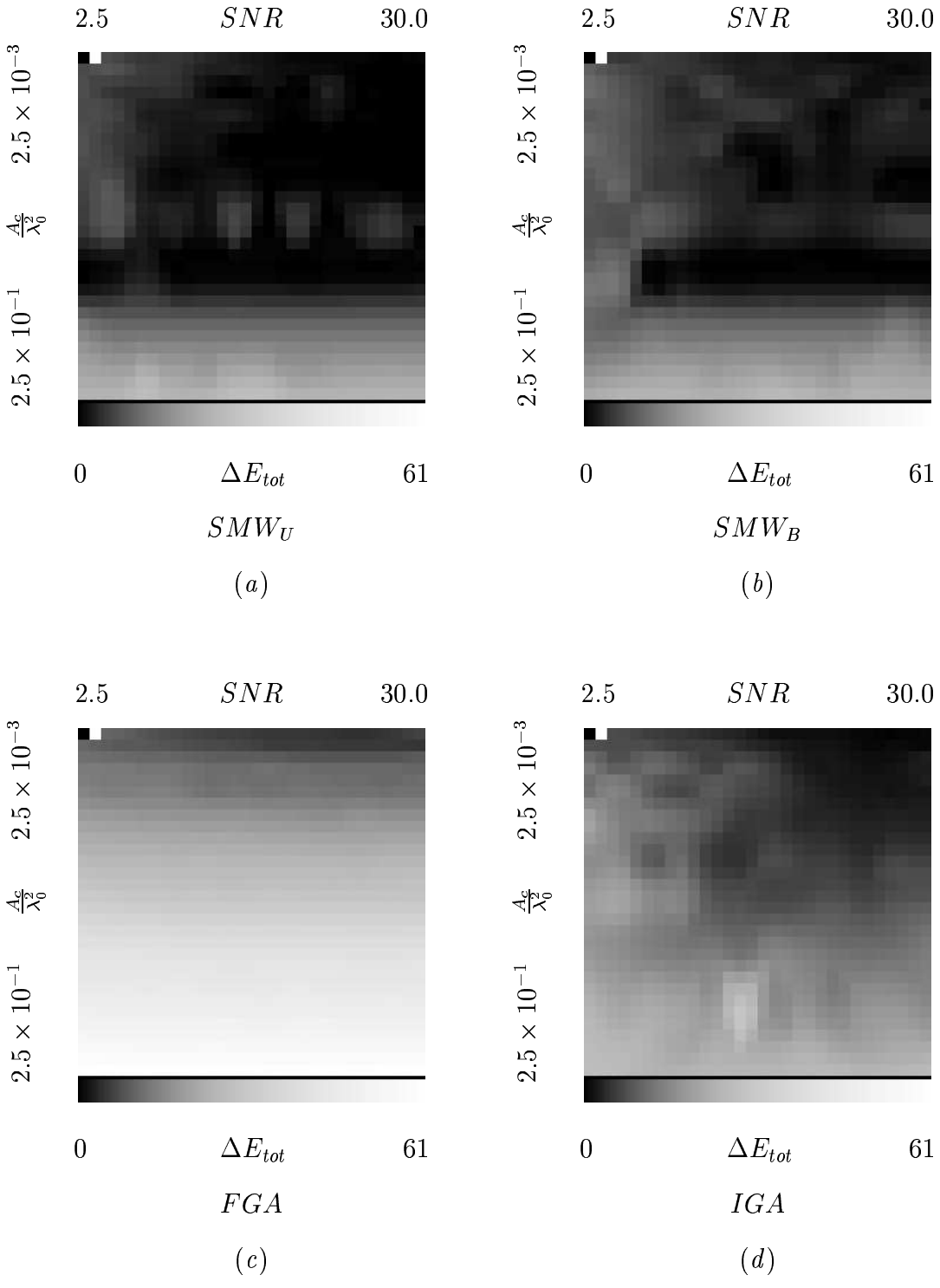

Fig. 7 - M. Benedetti *et al.*, "Effective Exploitation of the *A-Priori* Information ..."

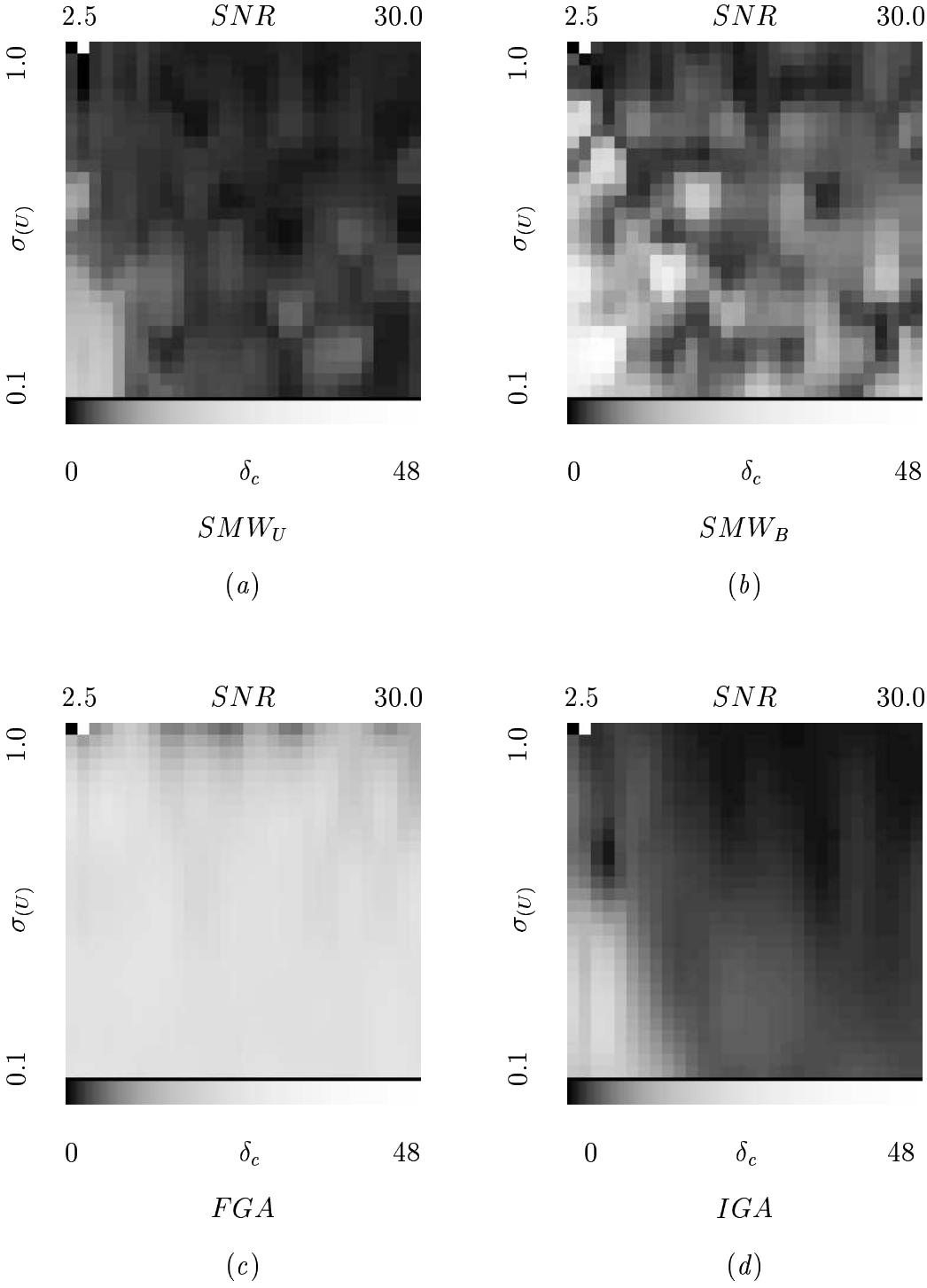

Fig. 8 - M. Benedetti *et al.*, "Effective Exploitation of the *A-Priori* Information ..."

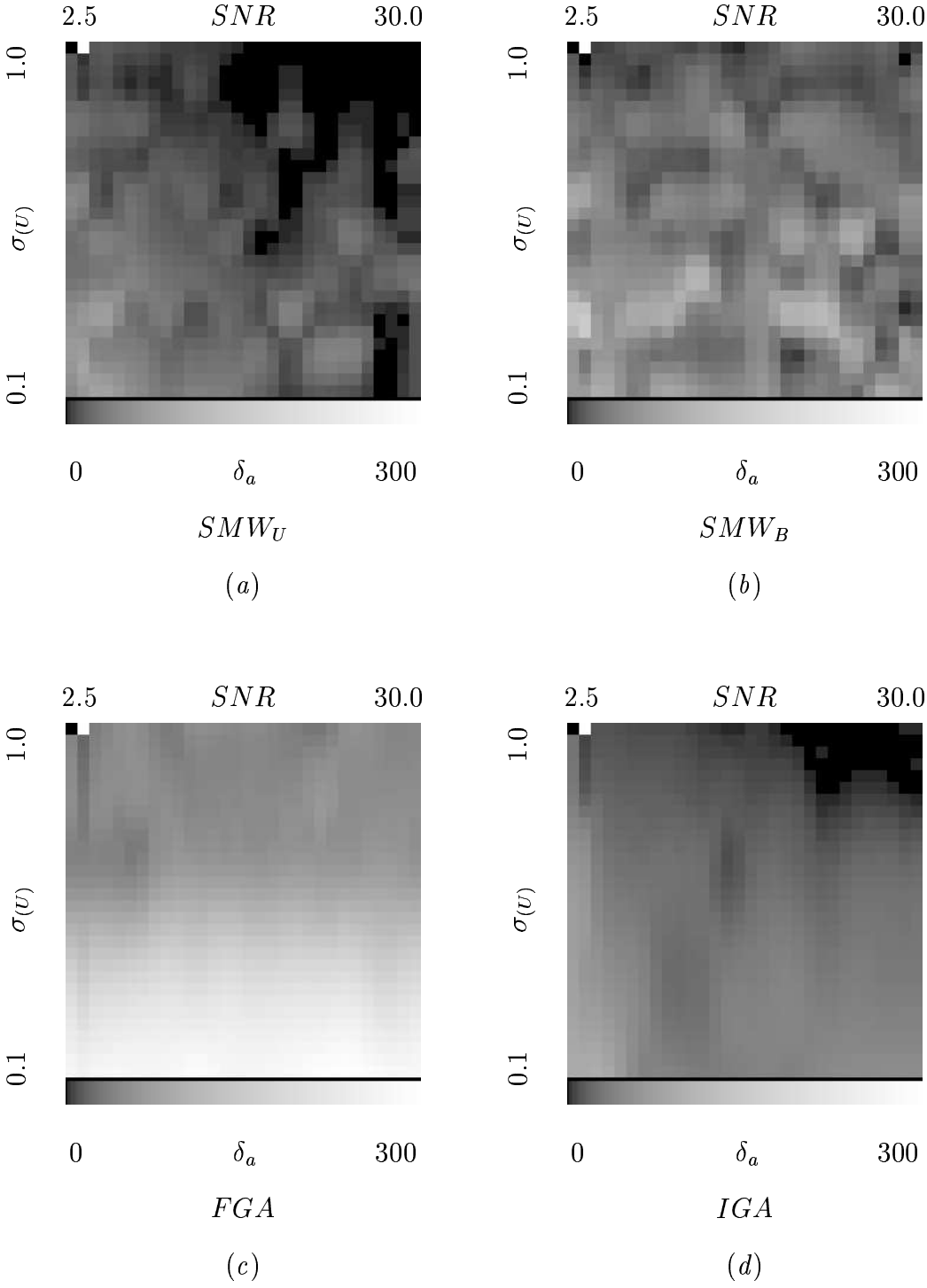

Fig. 9 - M. Benedetti *et al.*, "Effective Exploitation of the *A-Priori* Information ..."

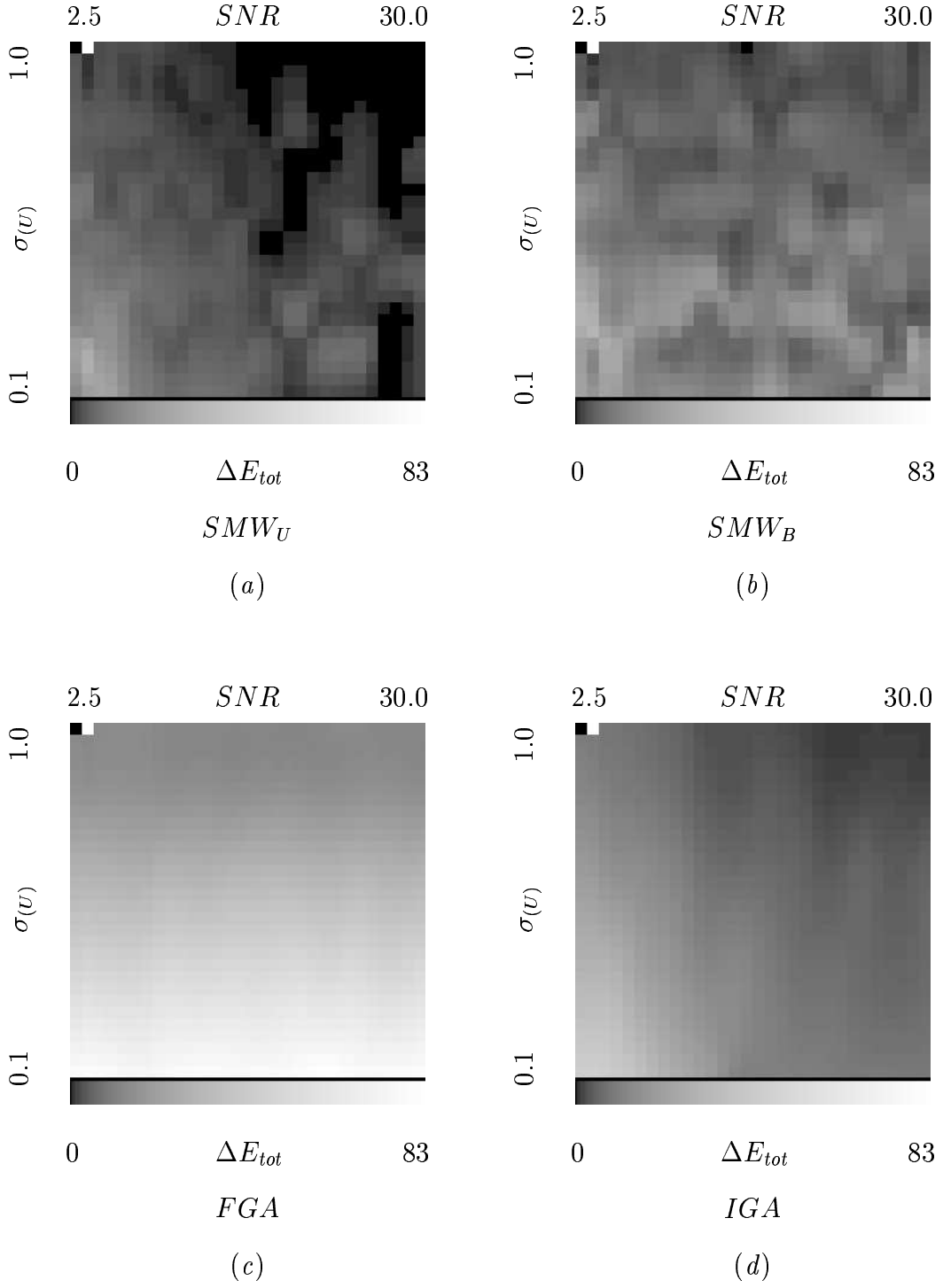

Fig. 10 - M. Benedetti *et al.*, "Effective Exploitation of the *A-Priori* Information ..."

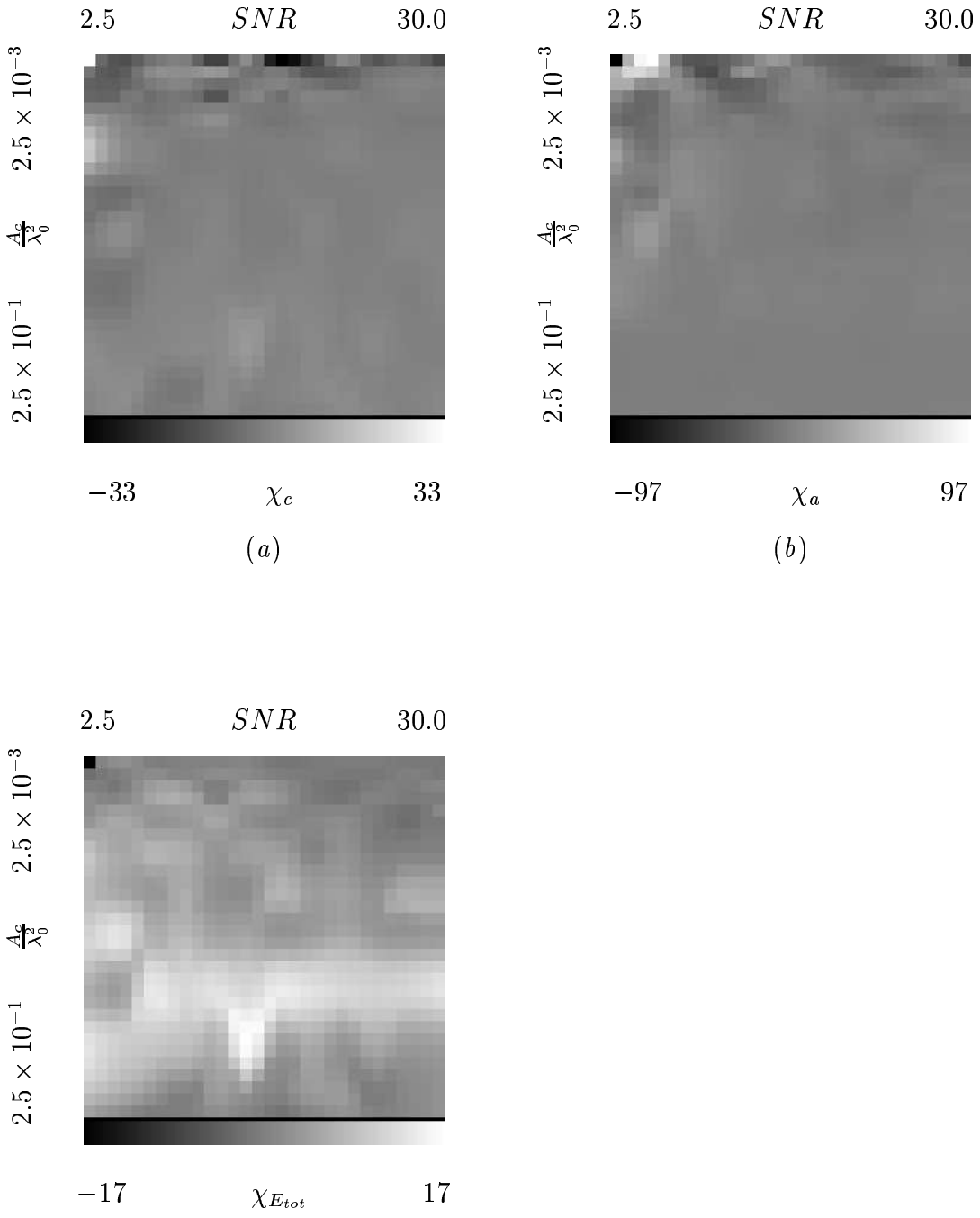

Fig. 11 - M. Benedetti *et al.*, "Effective Exploitation of the *A-Priori* Information ..."

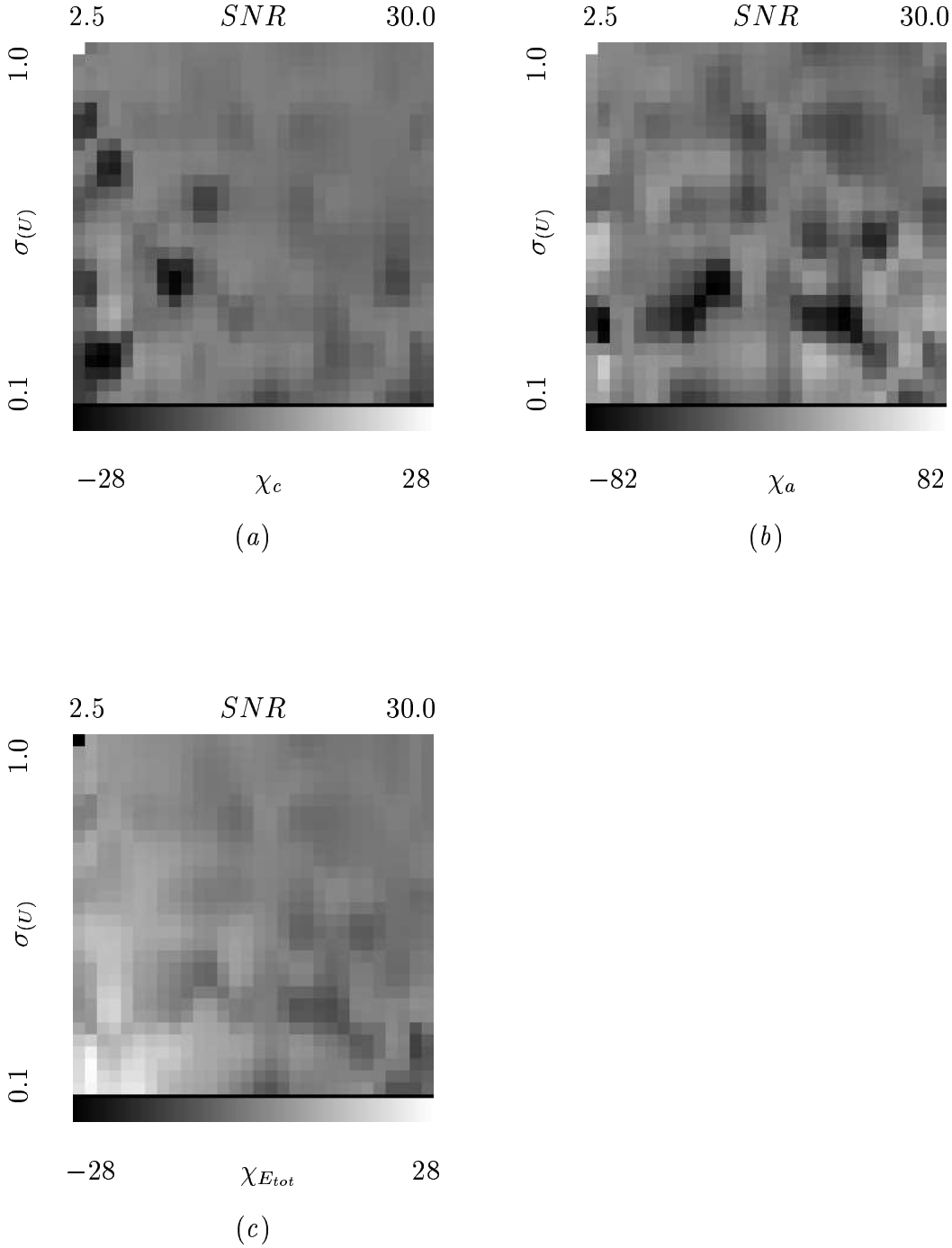

Fig. 12 - M. Benedetti *et al.*, "Effective Exploitation of the *A-Priori* Information ..."

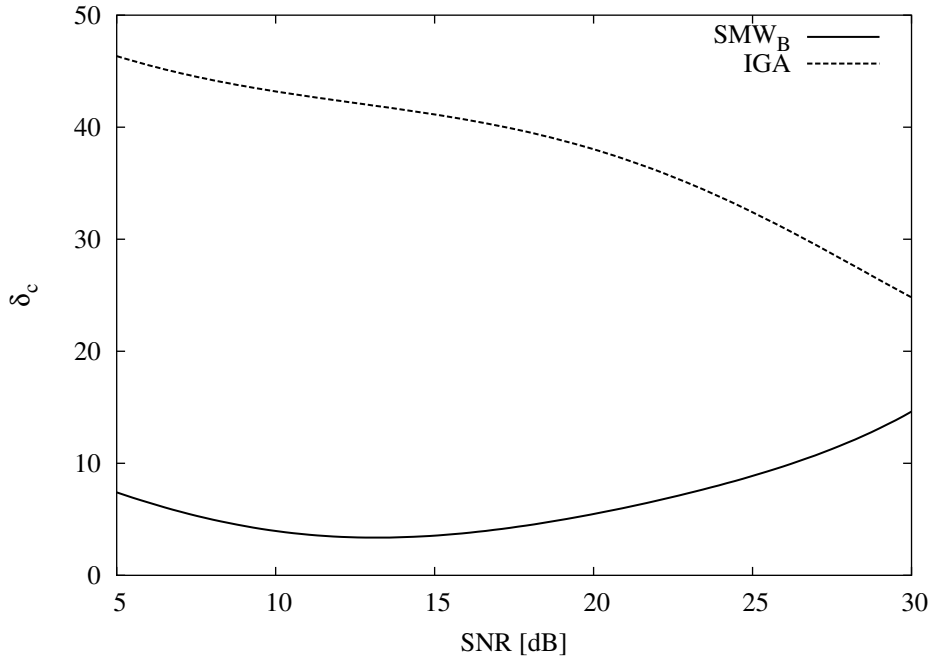

(a)

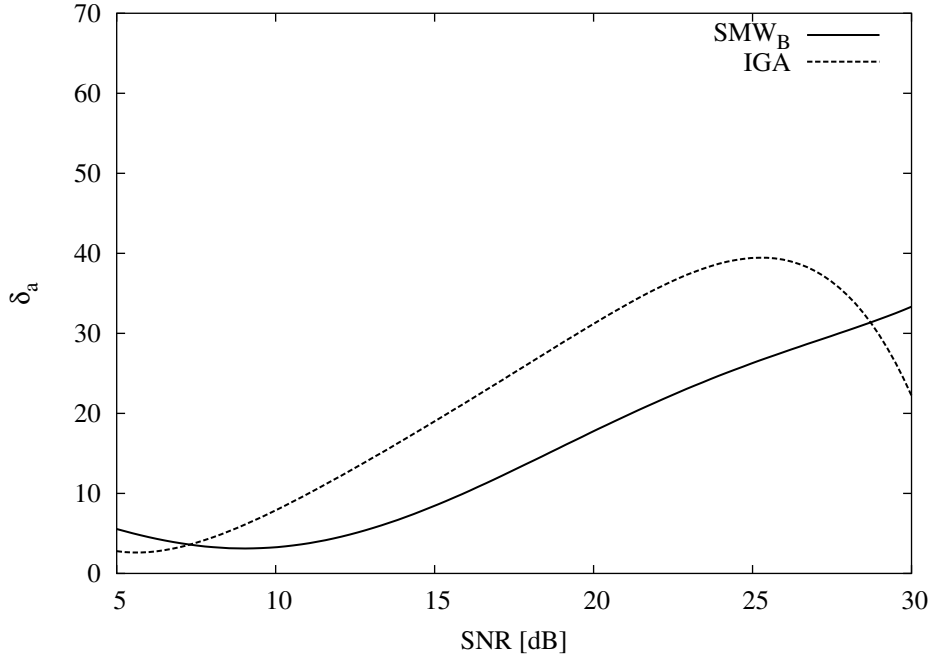

(b)

Fig. 13 - M. Benedetti *et al.*, "Effective Exploitation of the *A-Priori* Information ..."